Chemical Science

Accepted Manuscript

This article can be cited before page numbers have been issued, to do this please use: C. Li, Z. Huang, T. Li, T. Zhao, L. Zhou, Z. He, H. Tian and X. Ma, *Chem. Sci.*, 2026, DOI: 10.1039/D6SC02475K.

ROYAL SOCIETY OF CHEMISTRY

rsc.li/chemical-science

View Article Online
DOI: 10.1039/D6SC02475K

ARTICLE

Aromatic Phosphonate-Based Luminophores: Universal Building Blocks for Ultralong Room-Temperature Phosphorescence and Multifunctional Applications

Received 00th January 20xx,
Accepted 00th January 20xx

DOI: 10.1039/x0xx00000x

Chunli Li, Zizhao Huang, Tao Li, Tengjiao Zhao, Lei Zhou, Zhenyi He*, He Tian, and Xiang Ma*

The construction of organic ultralong room-temperature phosphorescence (OURTP) materials with high photoluminescence quantum yield and longevity is significant but challenging. Non-radiative transition caused by molecular excessive aggregation and vibrational relaxation usually suppresses phosphorescence of polycyclic aromatic hydrocarbons (PAHs) under ambient condition. Herein, functionalization of PAHs with diethyl phosphonate has been proven effective in achieving full-color OURTP with stimulus-responsive properties in various polymers. The introduction of hydrophilic substituent significantly inhabits molecular excessive aggregation and phase separation between host and guest. Non-covalent interactions such as hydrogen bonding and electrostatic interaction can enhance environmental rigidity and hinder vibrational relaxation. Synergistic effect of these interactions greatly suppresses non-radiative transition, unlocking efficient OURTP with longevity and high photoluminescence quantum yield of 2.05 s and 41.7% in different doped systems, respectively. Meanwhile, aromatic phosphonate-based luminophores can be uniformly dispersed in host by switching different hydrophilic and hydrophobic polymers. The extraordinary luminescence performance of doped systems outperforms other substituents, demonstrating the effectiveness and versatility of diethyl phosphonate functionalization. Furthermore, benefiting from the multi-stimulus response and full-color afterglow of doped systems, potential applications in anti-counterfeiting, dynamic pattern visualization and 3D printing are explored, providing novel perspectives for the construction and application in OURTP materials.

Introduction

Organic ultralong room-temperature phosphorescence (OURTP) materials, with unique attributes of long lifetime, large Stokes shifts and excellent modifiability, are attracting tremendous attention in advanced functional materials like biomedicine, anti-counterfeiting and photodynamic therapy.[1-8] The luminescence lifetime, photoluminescence quantum yield and color are usually considered as important performance parameters in practical application. However, the improvement of performance is primarily constrained by two factors. On the one hand, weak spin-orbit coupling (SOC) leads to low intersystem crossing (ISC) efficiency;[9] On the other hand, sensitive triplet excitons are prone to deactivation due to energy transfer with oxygen and flexible environment.[10] Traditionally, lanthanide metals and heavy atoms are introduced to promote ISC and generate triplet excitons while often suffers from drawbacks including great biotoxicity, high cost and limited processability. Notably, polycyclic aromatic hydrocarbons (PAHs) are viewed as promising and efficient organic luminophores. The large conjugated structure and rigid planar conformation provide possibility for high-performance RTP by reducing non-radiative transition. Furthermore, the modifiability of structure and tunability of electronic distribution can confer diversity in molecular structure, dynamic luminescence and functional applications.[11,12] Although PAHs can launch strong fluorescence, phosphorescence is typically suppressed at room-temperature for non-radiative transition caused by aggregation-caused quenching (ACQ).[13-15] Usually, useful strategies for enhancing environmental rigidity consist of crystallization, polymerization, host-guest complexation and doping.[16-18] Therein, polymer-based OURTP doped materials display promising potential in fields of flexible luminescence materials due to straightforward preparation, minimal dosage of luminophores, excellent flexibility and processability.[19,20]

Host polymers such as polymethyl methacrylate (PMMA) and polyacrylonitrile (PAN) exhibit pronounced hydrophobic properties, that necessitating guest molecular with oil solubility to ensure uniform dispersion for suppressing ACQ.[21,22] Nevertheless, oil-soluble luminophore often happen excessive aggregation in hydrophilic polymers like polyvinyl alcohol (PVA) for difference between hydrophilicity and hydrophobicity, which would enhance intermolecular π-π stacking and non-radiative transition, thereby triggering phase separation and significantly reducing luminescence properties.[23-25] Through precise molecular engineering, hydrophilic functional groups are introduced into PAHs to build local hydrophilic microenvironment, thereout preventing the occurrence of excessive aggregation and phase separation. Simultaneously, hydrophilic group including heteroatoms such as phosphorus and oxygen could

Key Laboratory for Advanced Materials and Joint International Research Laboratory of Precision Chemistry and Molecular Engineering, Frontiers Science Center for Materiobiology and Dynamic Chemistry, School of Chemistry and Molecular Engineering, East China University of Science and Technology, Shanghai 200237, China. E-mail: maxiang@ecust.edu.cn; zhenyiheh@qq.com

serve as excellent hydrogen bond acceptors to form strong hydrogen bond and stabilize triplet excitons.[26-31] The introduction of hydrophilic functional group enables researchers to design structure at molecular level and endows OURTP materials with extended functional properties, holding great promise for developing high-performance OURTP system.

Here, aromatic phosphonate-based luminophores were doped in various polymers by physical doping to successfully construct high-performance OURTP materials with stimulus-responsive and full-color tunability. With the change of molecular conjugation, different doped system achieved broadband OURTP emission spanning from blue to red.[32-34] Luminous lifetime and photoluminescence quantum yield of different doped systems reached up to 2.05 s and 41.7%, respectively. Meanwhile, doped systems exhibited stimulus-responsive characteristics to temperature, photoactivation and excitation wavelength. By switching host between hydrophilic and hydrophobic polymers, results showed that doped system containing aromatic phosphonate-based luminophores exhibited uniform luminescence, with superior luminescence performance compared to doped systems with other substituent groups. Analysis revealed that local hydrophilic microenvironment substantially suppresses ACQ caused by excessive aggregation of luminophores and phase separation.[35-38] At the same time, non-covalent interactions such as hydrogen bonding and electrostatic interaction between host and guest can strengthen the environment rigidity and inhibit vibrational relaxation.[39-42] Synergistic effects of these interactions greatly promoted high-performance OURTP. Efficient luminescent properties enable doped systems to possess great application potential in information encryption, anti-counterfeiting and 3D printing, paving a viable pathway for developing innovative and high-performance luminescent materials.

Results and discussion

View Article Online
DOI: 10.1039/D6SC02475K

A series of aromatic phosphonate-based luminophores were synthesized via one-step reaction, named BPP, NaP, PheP and PyP. The structures of luminophores were characterized by ^{1}H NMR, ^{13}C NMR and high-resolution mass spectroscopy (Fig. S1-S12†). High-performance liquid chromatography (HPLC) was employed to determine the purity of luminophores, thus avoiding the luminescence effect of impurities (Fig. S13 †). The 2-methyltetrahydrofuran solutions of four luminophores all exhibited distinct delayed emission at 77 K, indicating that four luminophores have giant potential for achieving OURTP in rigid environment at ambient condition[43] (Fig. S14†). Subsequently, PVA was selected as host matrix whose molecular chain contains abundant hydroxyl group (-OH) allowing solid hydrogen-bond formation with luminophores.[44-47] Doped systems were obtained by simply mixing luminophores and host in a 323 K aqueous solution followed by solvent evaporation and thermal annealing at 393 K for 30 minutes, termed BPP-PVA, NaP-PVA, PheP-PVA and PyP-PVA (Scheme 1).

The luminescence behaviours of doped systems with different doping mass concentration were investigated first (Fig. S15-S17†). Results suggested that doped systems maintained strong OURTP even at low mass concentration as 0.01 wt%. As the doped mass concentration increased, emission peak and absorption spectra of four doped systems all showed a gradual red shift trend (Fig. S18†). The UV-Vis absorption spectroscopy of four luminophores were recorded in Fig. S19. Taking luminescence intensity and lifetime of doped system into consideration, optimal doping mass concentrations were determined to be 0.1 wt% for BPP-PVA and PheP-PVA, and 0.3 wt% for NaP-PVA and PyP-PVA, respectively.

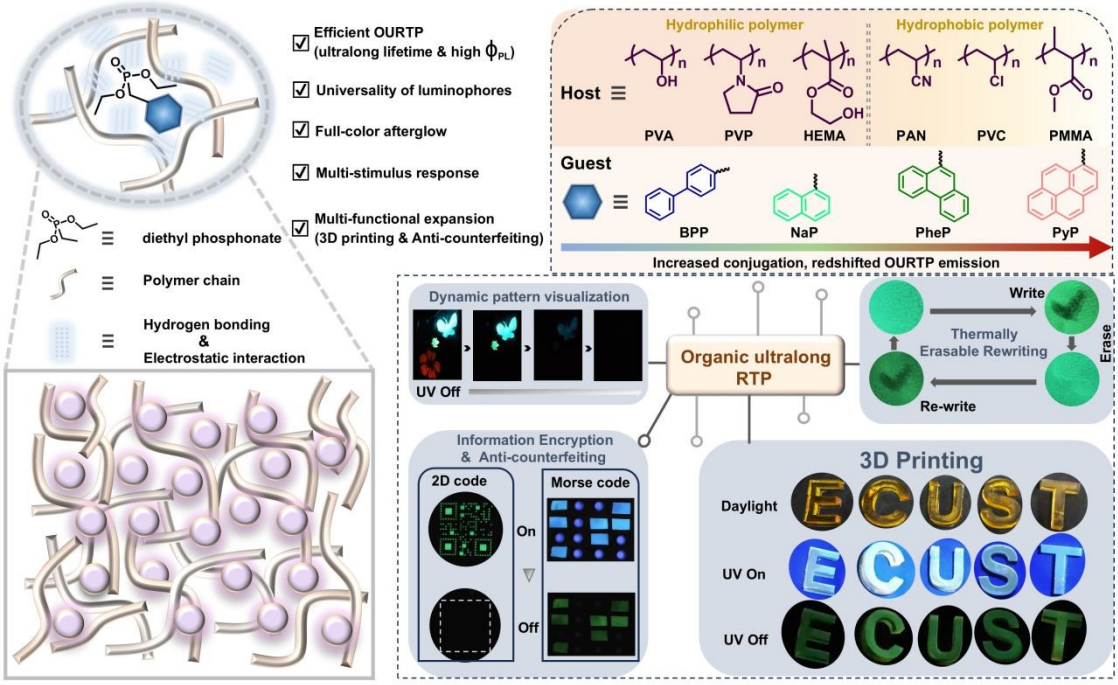

Scheme 1 Schematic illustration of the doped systems, molecular structures and applications.

View Article Online
DOI: 10.1039/D6SC02475K

ARTICLE

Four doped systems BPP-PVA, NaP-PVA, PheP-PVA and PyP-PVA displayed an obvious fluorescence peak around 320 nm, 340 nm, 373 nm and 396 nm, respectively (Fig. S20†). As shown in Fig. 1a, the delayed emission spectra of four doped systems displayed emission peak at 480 nm, 525 nm, 510 nm and 605 nm at room temperature, respectively. Luminescence color spanned the entire visible spectrum from blue to red, and corresponding lifetime of delayed emission reached up to 2.05 s, 1.26 s, 1.94 s and 0.32 s (Fig. 1b). Upon cessation of UV light, four films all exhibited long-lived bright emission, manifesting as visible afterglow (Fig. 1f). Both the long lifetime and large Stokes shift verified the phosphorescence properties of delayed emission in four doped systems.[48-50] Moreover, low temperature can suppress non-radiative transition led by free molecular motion, thereby resulting in reinforced emission intensity and longer lifetime.[51,52] For BPP-PVA, the lifetime of delayed emission at 480 nm extended from 0.14 s to 2.92 s accompanied with an increasing tendency of emission intensity when the temperature declined from 317 K to 77 K. This phenomenon could be viewed as typical phosphorescence property of four doped systems (Fig. 1d-1e).

It was worth noting that delayed emission peaks of BPP-PVA, NaP-PVA and PyP-PVA at room-temperature also correspond to delayed emission spectra of luminophores in dilute solutions at 77 K (Fig. S14 †), confirming that delayed emission originated form intrinsic phosphorescence of individual luminophore.[53] After cessation of ultraviolet (UV) irradiation, four doped systems exhibited visible long afterglow with different color. Besides, the afterglow duration of BPP-PVA and PheP-PVA exceeded 10 s (Fig. 1f). Photoluminescence quantum yields of doped systems were recorded in Fig. 1c, revealing that BPP-PVA, NaP-PVA, PheP-PVA and PyP-PVA exhibited efficient yields up to 15.9%, 9.0%, 21.4% and 41.7%, respectively. These results demonstrated the feasibility of diethyl phosphonate functionalization and then luminophores were incorporated into PVA rigid matrix to obtain excellent OURTP materials with long lifetime and high photoluminescence quantum yield.

To gain deeper insight into the luminescence mechanism of efficient OURTP in doped systems, relevant characterization and theoretical calculations were performed on four doped systems. Firstly, X-ray powder diffraction (XRD) was used to analyse the microstructure of doped systems. The results showed no obvious crystal characteristics and verified amorphous states of doped systems (Fig. 2a).

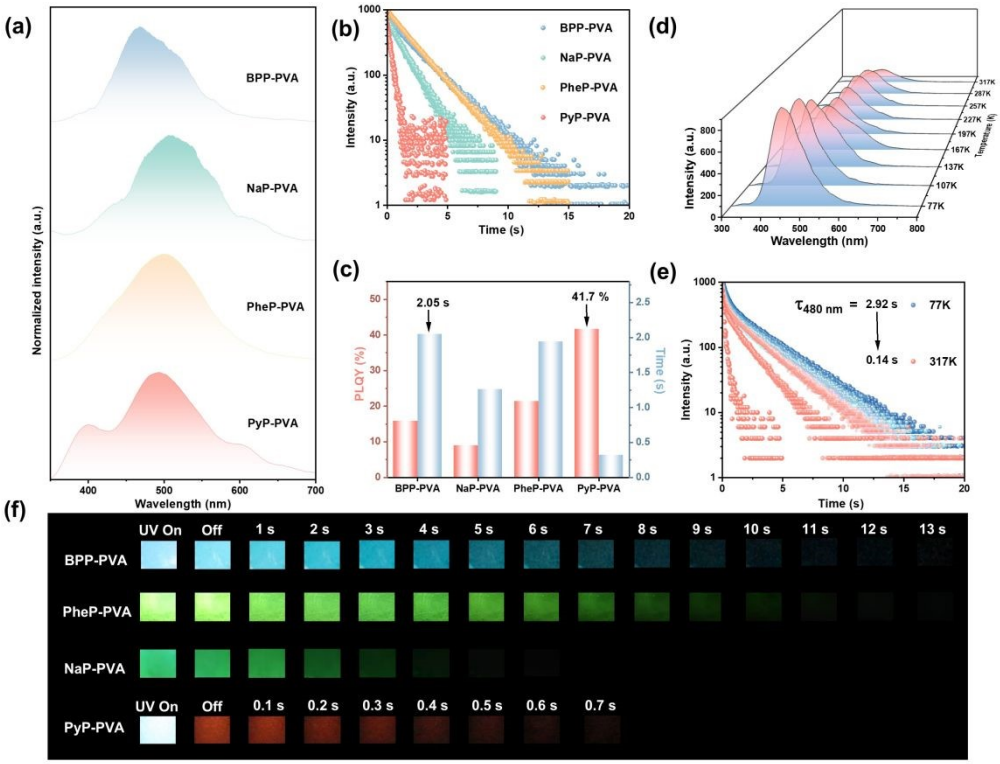

Fig. 1 (a) Delayed emission spectra and (b) Lifetime decay curves of BPP-PVA (λ_{ex} = 254 nm), NaP-PVA (λ_{ex} = 280 nm), PheP-PVA (λ_{ex} = 250 nm) and PyP-PVA (λ_{ex} = 305 nm); (c) Photoluminescence quantum yield and phosphorescence lifetime values of doped systems; (d) Temperature-dependent delayed emission and (e) lifetime decay curves of BPP-PVA (λ_{ex} = 254 nm); (f) Photographs of the luminescence of doped systems (delay time = 0.1 ms).

View Article Online
DOI: 10.1039/D6SC02475K

ARTICLE

Given that doped systems were amorphous, we speculated that efficient OURTP was promoted by non-covalent interactions between PVA matrix and luminophores, such as hydrogen bonding and electrostatic interaction. Therefore, fourier transform infrared (FT-IR) test was employed to confirm our hypothesis. PheP-PVA was selected as the research example. The vibration peak of -OH group located at 3253 cm^{-1} in pure PVA matrix. However, the vibration peak of film doped with 0.1 wt% PheP shifted to 3267 cm^{-1}. Then, the doping mass concentration of PheP was gradually increased to 10 wt%, -OH vibration peak of PheP-PVA underwent 24 cm^{-1} displacement and shifted to 3277 cm^{-1}, which clearly demonstrated the hydrogen bonding between PVA matrix and luminophores[54] (Fig. 2d). Furthermore, differential scanning calorimetry (DSC) analysis showed that the glass transition temperature in pure PVA matrix was 100.74 ℃, while doped system PheP-PVA displayed a higher glass transition temperature, implying the appearance of strong interactions occurred in PVA chain and luminophores[55] (Fig. 2b). Additionally, PAHs without diethyl phosphonate functionalization were doped in PVA matrix, named Na-PVA, BP-PVA, Phe-PVA and Py-PVA, and we tested the corresponding photophysical properties. Compared with films doped with aromatic phosphonate-based luminophores, doped films without diethyl phosphonate functionalization significantly exhibited lower photoluminescence quantum yield and shorter lifetime (Fig. 2e and S21 †). This was because atom P and O in diethyl phosphite could form hydrogen bonding with -OH in PVA chain, thereby inhibiting non-radiative transition induced by free molecular motion and enhancing phosphorescence performance[56] (Fig. 2c).

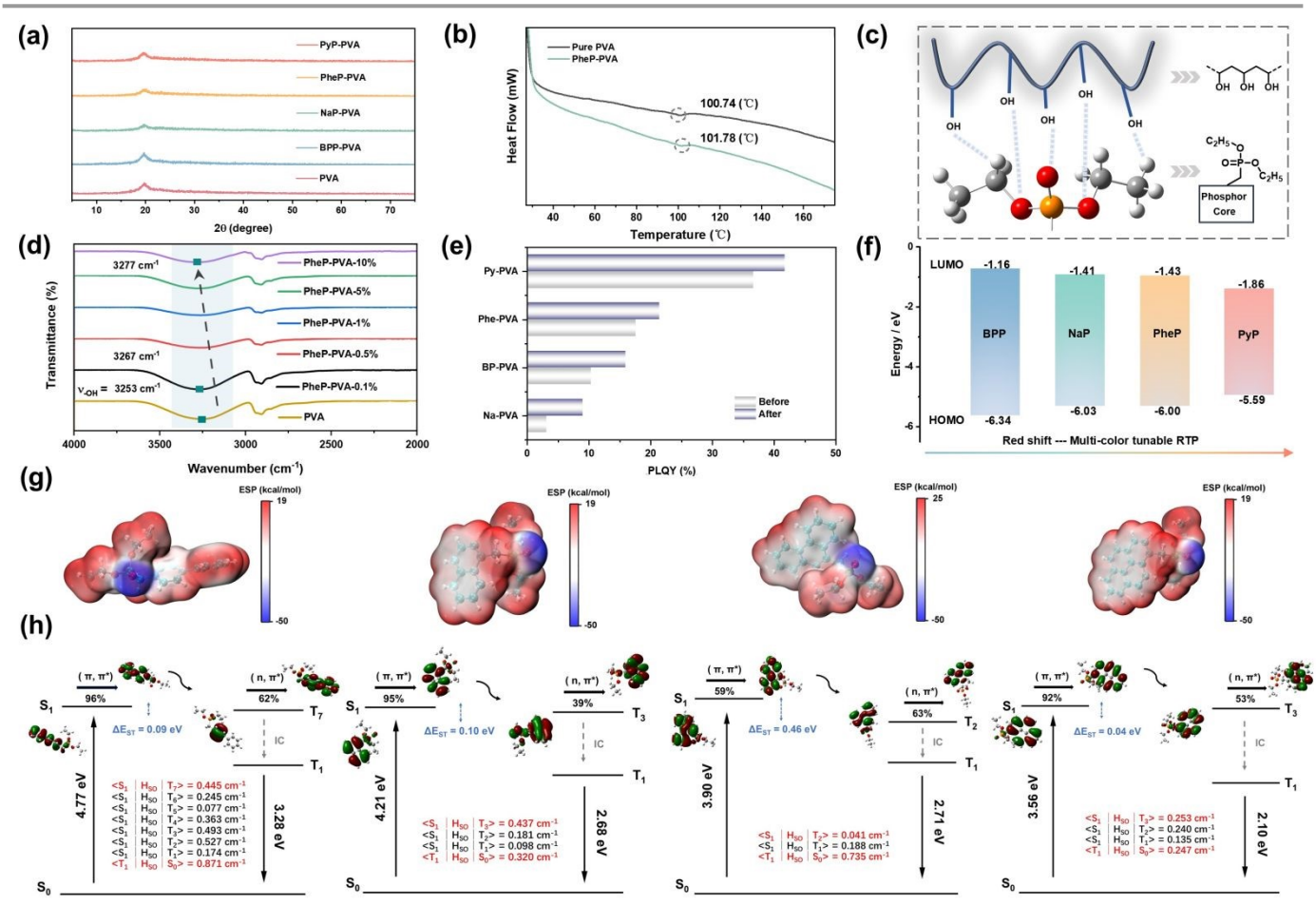

Fig. 2 (a) Powder XRD patterns of BPP-PVA, NaP-PVA, PheP-PVA and PyP-PVA; (b) DSC of pure PVA and PheP-PVA; (c) Brief illustration of hydrogen bonding; (d) FT-IR spectra of PVA and PheP-PVA with different mass ratio of luminophore; (e) Photoluminescence quantum yield of doped systems before and after diethyl phosphonate functionalization; (f) Frontier molecular orbital analysis, (g) ESP distribution and (h) Energy level distributions of BPP, NaP, PheP and PyP.

View Article Online
DOI: 10.1039/D6SC02475K

ARTICLE

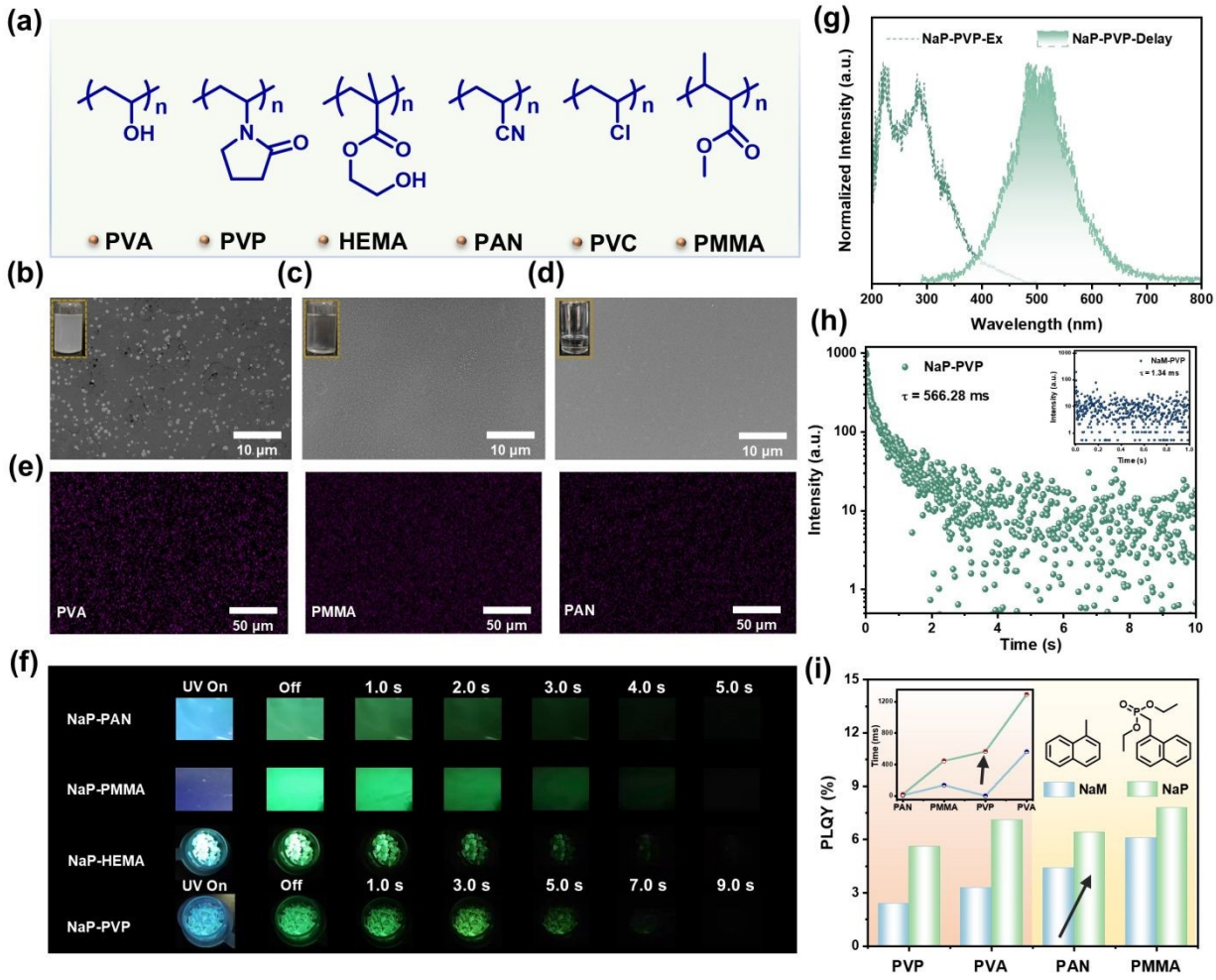

Fig. 3 (a) Chemical structure of polymers; SEM images of (b) NaM-PVA, (c) NaP-PVA and (d) NaP-PMMA; (e) EDS mapping of P element in doped systems; (f) Photographs of luminescence of doped systems; (g) Excitation spectra and Delayed emission spectra of NaP-PVP; (h) Lifetime decay curves of NaM-PVP (λ_{ex} = 280 nm) and NaP-PVP (λ_{ex} = 280 nm); (i) Photoluminescence quantum yield and lifetime of doped systems. All test were conducted at 25 ℃ under ambient condition.

Meanwhile, density-functional theory calculations were applied to obtain the electrostatic potential (ESP) distributions on the surfaces of PVA and four luminophores for characterizing electrostatic interaction (Fig. 2g). Four luminophores exhibited negative ESP values in phosphine carbonyl moieties, which can be attributed to the strong electron-withdrawing capability. In contrast, the hydrogen atoms of the -OH groups in pure PVA demonstrated strong electron-donating ability due to the electron push-pull effect (Fig. S22†). When luminophores contacted PVA chains in the doping environment, strong electrostatic interaction would happen for the existence of phosphine carbonyl moiety with electron-withdrawing capability was complementary to the electron-donating portion in PVA chain.[57,58] Microenvironment around luminophores became more rigid, that helped reduce non-radiative transition and prolonged lifetime.

At the same time, density-functional theory (DFT) and time-dependent density-functional theory (TD-DFT) calculations were also used to evaluate the ground-state and excited-state geometry, the highest occupied molecular orbital (HOMO)-lowest unoccupied molecular orbital (LUMO) and energy level distributions. From the perspective of electronic conformation, the S_1 states of four luminophores were dominated by π-π* transitions from HOMO to LUMO (Fig. 2h). For luminophore PheP, 63% n-π* transition appeared in T_2 level. BPP exhibited 62% n-π* transition in T_7 level.

According EI-sayed rule,[59] the appearance of different transition is permitted. Hence luminophores had giant potential for achieving efficient OURTP. Data revealed that NaP exhibited an energy gap of 0.0995 eV from S_1-T_1 with a SOC constant of 0.437 cm^{-1}. Smaller singlet-triplet energy gap and larger SOC constant of aromatic phosphonate-based luminophores led to pronounced ISC process and promoting OURTP performance[27] (Fig. 2f and Table S1†). HOMO-LUMO energy gap of BPP and PyP was 5.18 eV and 3.73 eV, respectively. The gradually decreasing energy gaps of HOMO-LUMO from BPP to PyP simultaneously demonstrated that OURTP of doped systems can be redshifted from blue to red, spanning the visible spectrum[7] (Fig. 2f). The energy gap of four luminophores without diethyl phosphonate functionalization showed the same trend and theoretical calculations are consistent with experimental phenomenon (Fig. S23†). Therefore, the rigid environment formed by strong non-covalent interactions between PVA matrix and aromatic phosphonate-based luminophores was responsible for efficient OURTP. Besides, PheP was selected as template molecule to be doped into various host matrices. Experimental results revealed that doped systems containing PheP still exhibited long and efficient OURTP (Fig. S24-S25†), further verifying the universal applicability of aromatic phosphonate-based luminophores across different host matrices.

The planar conjugated structure of unmodified PAHs endows molecule with appreciable rigidity and potential of achieving efficient OURTP with full-color tunability. Whereas, the hydrophobic nature frequently triggers phase separation when luminophores were dispersed in hydrophilic polymer, thus leading excessive aggregation, non-radiative transition caused by π-π stacking and quenching phosphorescence.[11] Therefore, molecular engineering was employed to modify PAHs with diethyl phosphonate. The polarity of diethyl phosphonate enabled luminophores to form hydrogen bonding with water molecules, creating local hydrophilic microenvironment. The presence of ethyl group also increased steric hindrance, urging more dispersed distribution of luminophores in host and improvement of phosphorescence performance.

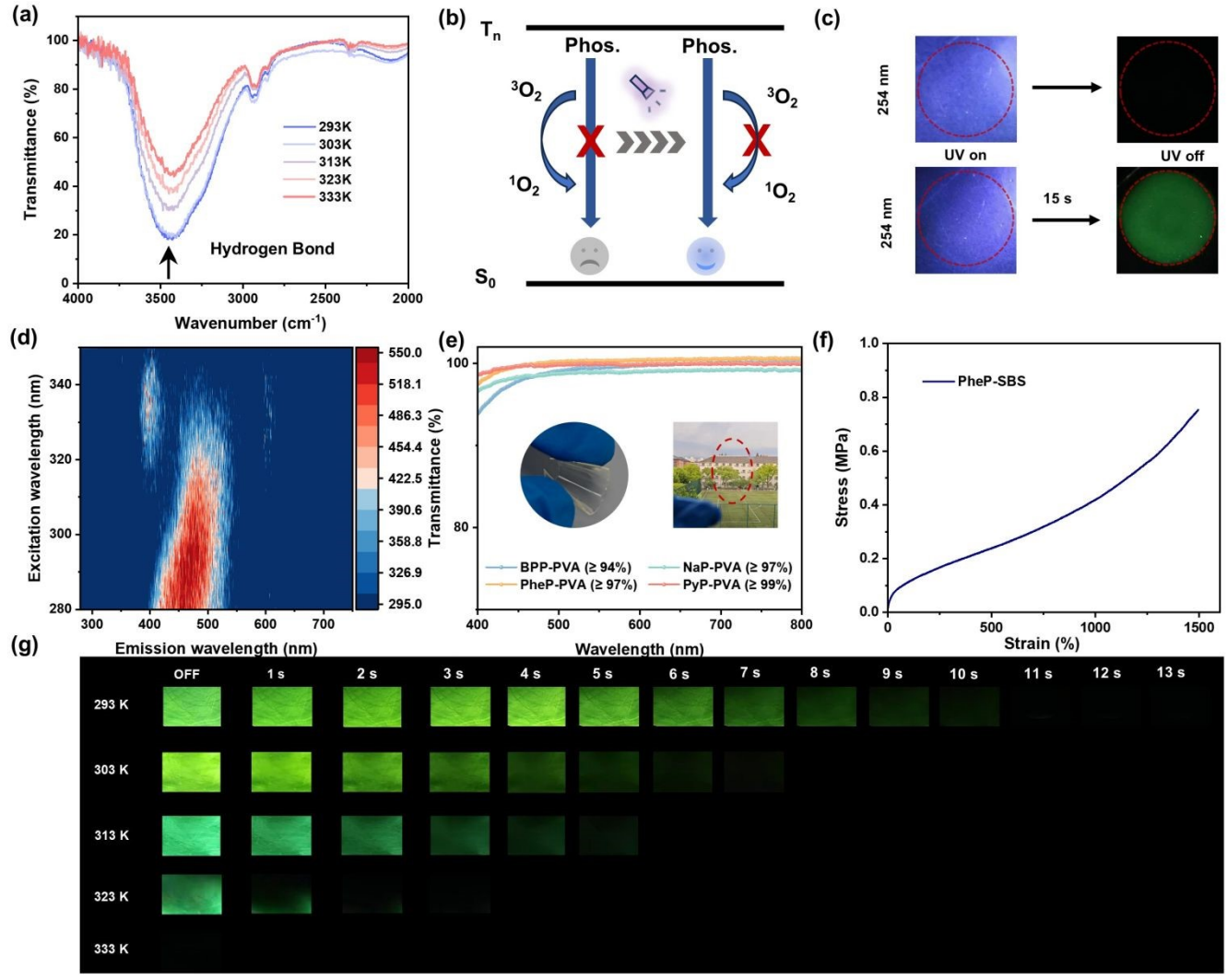

Fig. 4 (a) Temperature-dependent FT-IR spectra and (g) Afterglow Photographs of PheP-PVA (λ_{ex} = 254 nm); (b) The diagram of internal mechanism of oxygen consumption and (c) Photographs of PheP-PMMA under UV irradiation; (d) Excitation-emission mapping of PyP-PVA; (e) Transmittance spectra of BPP-PVA (thickness = 0.10 mm), NaP-PVA (thickness = 0.10 mm), PheP-PVA (thickness = 0.10 mm) and PyP-PVA (thickness = 0.10 mm). Inset: Photographs of NaP-PVA; (f) The stress-strain curves of PheP-SBS.

View Article Online
DOI: 10.1039/D6SC02475K

ARTICLE

To verify the rationality of diethyl phosphonate functionalization, luminophores named NaM without diethyl phosphonate functionalization was doped in both hydrophilic and hydrophobic polymers to make a comparation with doped system containing NaP (Fig. 3a). The fluorescence spectra and photoluminescence spectra of NaM solution both displayed obvious emission peak around 305 nm. But NaM solution showed no delayed emission under ambient condition, that was caused by the relatively low rigidity of environment and quenching effect of water and oxygen (Fig. S26†). The UV-vis absorbance spectra of NaM solution was presented in Fig. S27. Moreover, it could be seen that the distribution of NaM and NaP were uniform in hydrophobic polymer. For example, the mixture of NaP and PMMA was homogeneous and transparent after ultrasonication at 323 K for 1 h (Fig. 3d). After solvent evaporated tardily, the surface of doped systems appeared exceptionally smooth and flat. Energy-dispersive X-ray spectroscopy (EDS) images revealed uniform P distribution throughout doped systems without any excessive aggregation clumps (Fig. 3e). This result stemmed from the inherent lipophilic nature of benzene ring in luminophores, enabling uniform distribution of luminophores with hydrophobic host in organic solvent. In other hydrophobic host such as PAN and poly (vinyl chloride) (PVC), doped systems containing NaP all exhibited visible afterglow (Fig. 3f). Next, PVA, polyvinyl pyrrolidone (PVP) and poly (2-hydroxyethyl methacrylate) (HEMA) were selected as hydrophilic host. The mixture of NaM-PVA remained cloudy and opaque after ultrasonication at 323 K for 1 h (Fig. 3b). After solvent evaporated naturally, excessive aggregation clumps were observed in scanning electron microscopy (SEM) images, indicating uneven distribution of luminophores in PVA. But the mixed solution of NaP-PVA became homogeneous and transparent after ultrasonication at 323 K for 1 h (Fig. 3c). NaP-PVA exhibited smooth and uniform surface under SEM observation, with no large excessive aggregation clumps. EDS results revealed uniform distribution of P, implying concomitant diminution of phase separation and excessive aggregation happened in luminophores (Fig. 3e). Above results suggested that aromatic phosphonate-based luminophores displayed highly uniform dispersion and luminescence in both hydrophilic and hydrophobic polymers, avoiding phase separation and excessive aggregation of luminophores (Fig. S28†).

Subsequently, we tested delayed emission spectra and lifetime of 1-methylnaphthalene (NaM) and NaP by switching host. Delayed emission spectra of NaM and NaP in different host all displayed emission peak at 525 nm, with visible green afterglow at room-temperature. However, lifetime of systems doped NaP consistently exceeded those of systems doped NaM (Fig. S29-S32 †). Taking hydrophilic host PVP as an example, NaM-PVP showed short lifetime of 1.34 ms, whereas the lifetime of NaP-PVP reached up to 566.28 ms, prolonging by 422-fold (Fig. 3g and 3h). In hydrophobic host PMMA, NaP-PMMA exhibited long lifetime of 446.9 ms after photoactivation, while NaM-PMMA only showed a lifetime of 136.46 ms after photoactivation.

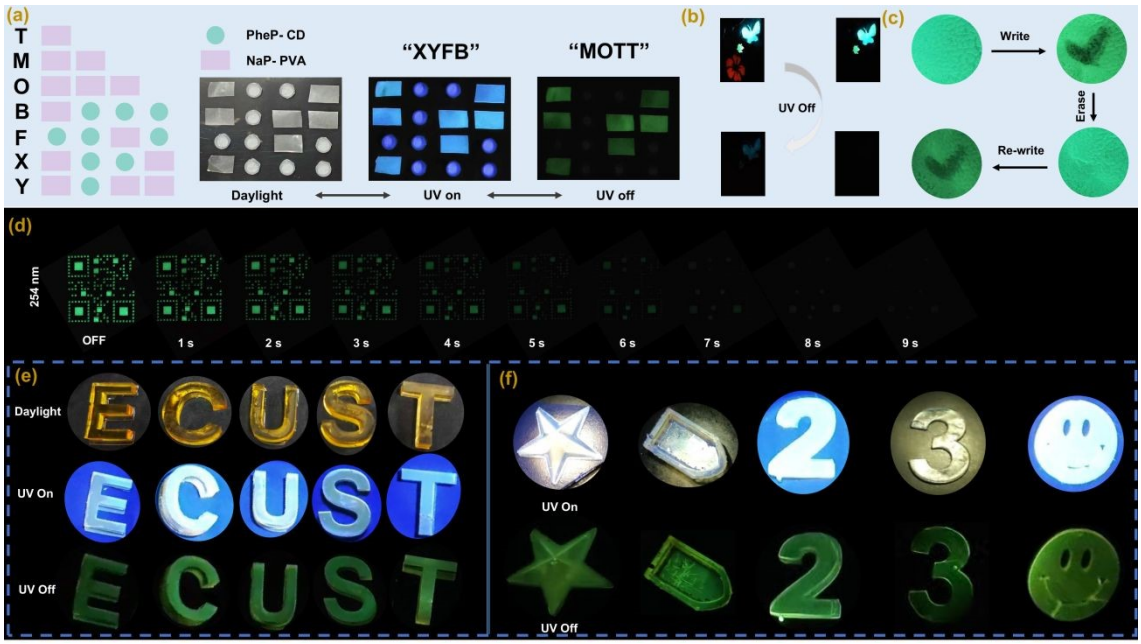

Fig. 5 (a) Information encryption with Morse code (PheP-CD and NaP-PVA); (b) Dynamic display of patterns (BPP-PVA, PheP-PVA and PyP-PVA); (c) Schematic illustration of application process for PheP-PVA rewritable doped system; (d) The 2D code imaging based on PheP-PVA; (e) and (f) Photographs of 3D RTP materials under daylight, UV excitation and after switching off.

View Article Online
DOI: 10.1039/D6SC02475K

ARTICLE

Furthermore, photoluminescence quantum yields of systems doped NaP were higher than that of systems doped NaM in both hydrophilic and hydrophobic polymers (Fig. 3i), implying that diethyl phosphonate functionalization prevented the excessive aggregation and benefited uniform distribution of luminophores in host. Consequently, synergistic effect of non-covalent interactions like hydrogen bonding and electrostatic interaction enhanced microenvironment rigidity, promoting OURTP performance in forms of lifetime and photoluminescence quantum yield.

Additionally, four different hydrophilic functional groups carboxyl (-CA), amino (-NH), sulfonic acid (-SA) and boric acid (-BA) were used to modified Na, named Na-BA, Na-SA, Na-CA and Na-NH. These luminophores were doped into PVA to construct doped films, and photophysical properties were analysed. Results showed that all doped films achieved obvious emission at 525 nm with lifetime below 1 s. Visible green afterglow was observable at room-temperature after turning off UV light. Comparing phosphorescence performance of these four doped systems with NaP-PVA, NaP exhibited the longest lifetime, and photoluminescence quantum yield was second only to that of Na-BA-PVA. These findings suggested that doped systems containing aromatic phosphonate-based luminophores afforded the overall best phosphorescence performance, surpassing other hydrophilic functional group-substituted luminophores[60] (Fig. S33 †). Given that non-covalent interactions were highly sensitive to environmental changes and can respond promptly, we investigated the stimulus-responsive properties of doped systems. The influence of temperature variation on the luminescence of doped systems was researched. As temperature increased from 293 K to 333 K, afterglow duration of PheP-PVA gradually decreased from 13 s (Fig. 4g). We speculated that high temperature would destroy hydrogen bonding between PVA and luminophores, reducing the rigidity of microenvironment around luminophores and declining phosphorescence performance. FT-IR test was employed to confirm this variation (Fig. 4a). Vibration peak of PheP-PVA at 3436 cm^{-1} indicated the appearance of hydrogen bonding between PVA and PheP. When temperature arose to 333 K, intensity of vibration peak diminished, and the position shifted to 3418 cm^{-1}. This change confirmed that hydrogen bonding between host and luminophores weaken with increasing temperature, reducing the rigidity of doped environment.[61] Acceleration of non-radiative transition directly led to the decline of OURTP.

Next, response property of PheP-PMMA on photoactivation was researched. After turning off UV light, PheP-PMMA without photoactivation showed no afterglow. Upon 15 s continuous photoactivation at 254 nm, PheP-PMMA exhibited vivid green afterglow after cessation of UV irradiation (Fig. 4b and 4c). It has been reported that PMMA can create relatively rigid microenvironment for luminophores, but are prone to oxygen permeation, which easily quenches triplet excitons and declines OURTP. To determine potential photoactivation mechanisms, delayed emission spectra of PheP-PMMA under argon and air were measured (Fig. S34 †). In air, PheP-PMMA showed no significant emission after stopping UV irradiation, and lifetime was difficult to detect. Nevertheless, PheP-PMMA under argon environment displayed strong emission peak at 510 nm after stopping UV irradiation. During the process of photoactivation, UV light would gradually deplete oxygen.[62] Then sensitive triplet excitons were successfully released and emitted phosphorescence.

It is well known that doped systems containing Py could represent concentration-dependent property.[63] As a result, PyP-PVA was chosen as research subject to explore phosphorescence performance. Upon increasing excitation wavelength, phosphorescence emission of PyP-PVA gradually underwent red shift (Fig. 4d). Analogous to concentration dependence, wavelength dependence of excitation originated from the formation of aggregates, causing overall red shift in excitation and emission wavelength of doped systems. Besides, doped films all owned high transparency and flexibility. For hydrophilic polymer PVA, the transmittance rate of PheP-PVA and NaP-PVA were as high as 97% among the range of 400 nm-800 nm, while PyP-PVA surpassed 99% (Fig. 4e). The doped films with hydrophobic polymer also exhibit high transparency. For instance, the transmittance rate of both NaP-PMMA and NaP-PVC exceeded 90% among the wavelength range above 400 nm (Fig. S35†). Furthermore, PheP showed favorable mechanical property in block-copolymer host like isoprene-styrene (SBS). PheP-SBS withstand tensile stress up to 0.75 MPa while sustaining elongations approaching 1500% (Fig. 4f). To sum up, different doped systems achieved efficient OURTP with high photoluminescence quantum yield and lifetime up to 41.7% and 2.05 s, respectively. Color covered visible spectrum from blue to red, and multi-stimulus response endowing the doped materials with broad application prospects.

Based on efficient OURTP of doped systems, we explored feasible application in field of information encryption. PheP-CD and NaP-PVA presented circular and rectangular shapes, respectively. Under daylight, we arranged the two doped materials in a specific sequence. Leveraging the different afterglow duration time of two doped materials after stopping UV irradiation, information was stored and encrypted with the aid of Morse code. Under UV light at 254 nm, PheP-CD and NaP-PVA both emitted blue fluorescence, storing information “XYFB”. Upon removing UV light, NaP-PVA blocks exhibited green afterglow, revealing real information “MOTT” (Fig. 5a). Otherwise, discrepancy of afterglow lifetime and color in doped systems were applied to dynamic pattern visualization. After removing UV light, red flowers, green leaves and blue butterflies could be observed. Due to the short afterglow of PyP-PVA, red flowers disappeared first, leaving only leaves and butterflies. With

time progressed, patterns of leaves and butterflies gradually dimmed until they vanished completely (Fig. 5b). We placed PheP-PVA film beneath QR code plate. Green QR code pattern became clear after the removal of UV light, and then faded overtime (Fig. 5d). Benefitting from sensitive nature of doped systems to temperature and water, we employed water ad ink for erasable writing on the surface of doped film. Pattern " √ " was written on the surface of PheP-PVA using water. Heating can erasure this pattern and this process was repeatable (Fig. 5c).

Using 3D printing technology, we uniformly dispersed NaP in thermosetting resin at low doping concentration and successfully fabricated 3D materials with OURTP properties. The letter "E", number "2" and five-pointed star pattern were printed, demonstrating the practical formability. Under UV irradiation, printed 3D structures all displayed spontaneous blue fluorescence. Turning off UV light, 3D structures showed green afterglow (Fig. 5e-5f). Thereout, doped materials with aromatic phosphonate-based luminophores hold great application potential in functional materials.

Conclusions

In summary, through physical doping, four aromatic phosphonate-based luminophores with distinct conjugated structure were respectively doped into various polymers to successfully construct efficient OURTP materials with multi-stimulus response and full-color tunability. The incorporation of hydrophilic diethyl phosphonate facilitated the formation of local hydrophilic microenvironment, preventing excessive aggregation and promoting uniform dispersion of luminophores. Meanwhile, vibrational relaxation was greatly suppressed by rigid environment induced by non-covalent interactions such as hydrogen bonding and electrostatic interaction. Consequently, synergistic effect of the two mechanisms was responsible for significant improvement of phosphorescence performance in doped systems. The high photoluminescence quantum yield of 41.7% and long lifetime up to 2.05 s could be simultaneously implemented in different doped systems. Profiting from local hydrophilic nature of aromatic phosphonate-based luminophores, molecule displayed excellent adaptability and uniform distribution in both hydrophilic and hydrophobic polymers, releasing high-performance OURTP. Furthermore, outstanding stimulus-response properties of doped systems on temperature, excitation wavelength and photoactivation enabled applications in anti-counterfeiting, dynamic pattern visualization and 3D printing promising. This work provides new insights for the construction and application expansion of high-performance OURTP materials.

Data availability

All the data are available in the ESI. †

Author contributions

C. Li, Z. He, H. Tian and X. Ma designed the materials and conceived the project. C. Li conducted the molecule synthesis and characterization. T. Li performed theoretical calculation. C. Li and X. Ma wrote the manuscript. All authors engaged in discussion and conducted data analysis.

Conflicts of interest

There are no conflicts to declare.

Acknowledgements

We gratefully acknowledge the financial support from the National Natural Science Foundation of China (22125803, T2488302, and 22408106), the Science and Technology Commission of Shanghai Municipality (24DX1400200), the Guangxi Department of Science and Technology (AA23062016), Shanghai Rising Star Program (24YF2708500), and the Fundamental Research Funds for the Central Universities.

References

1 C. Yin, Z. Wu, Z. Yan, P. Jiang, Y. Ding, T. Li, Y. Chen, H. Tian and X. Ma, *J. Am. Chem. Soc.*, 2025, **147**, 43286-43294.
2 W. Ye, H. Ma, H. Shi, H. Wang, A. Lv, L. Bian, M. Zhang, C. Ma, K. Ling, M. Gu, Y. Mao, X. Yao, C. Gao, K. Shen, W. Jia, J. Zhi, S. Cai, Z. Song, J. Li, Y. Zhang, S. Lu, K. Liu, C. Dong, Q. Wang, Y. Zhou, W. Yao, Y. Zhang, H. Zhang, Z. Zhang, X. Hang, Z. An, X. Liu and W. Huang, *Nat. Mater.*, 2021, **20**, 1539-1544.
3 X. Zhou, H. Zhang and Y. Liu, *Chem. Sci.*, 2024, **15**, 18259-18271.
4 N. Li, Y. Wang, S. Chen, J. Li and Z. Li, *Angew. Chem. Int. Ed.*, 2025, **64**, e202520504.
5 H. Hou, H. Wang, M. He, Q. Li, X. Wang, F. Guo, Q. Chen, L. Qu and C. Yang, *Angew. Chem. Int. Ed.*, 2024, **63**, e202411323.
6 X. Li, J. Li, G. Wang, Y. Su, M. Wu and K. Zhang, *Nat. Commun.*, 2025, **17**, 226.
7 Z. He, J. Song, C. Li, Z. Huang, W. Liu and X. Ma, *Adv. Mater.*, 2025, **37**, 2418506.
8 W. Zhao, Z. He and B. Tang, *Nat. Rev. Mater.*, 2020, **5**, 869-885.
9 Z. Yan, C. Yin, H. Tian and X. Ma, *Angew. Chem. Int. Ed.*, 2025, **64**, e202417397.
10 J. Cao, J. Song, Y. Hu, F. Zhang and X. Ma, *CCS Chem.*, 2025, **7**, 2065-2074.
11 Y. Liang, P. Hu, H. Zhang, Q. Yang, H. Wei, R. Chen, J. Yu, C. Liu, Y. Wang, S. Luo, G. Shi, Z. Chi and B. Xu, *Angew. Chem. Int. Ed.*, 2024, **63**, e202318516.
12 Y. Jiang, C. Zhang, R. Wang, Y. Lei, W. Dai, M. Liu, H. Wu, Y. Tao and X. Huang, *Adv. Optical Mater.*, 2024, **12**, 2302482.
13 H. Chen, Y. Zhang, J. Shan, M. Dong, Z. Qian, A. Lv, H. Qian, H. Ma, Z. An, L. Gu and W. Huang, *Angew. Chem. Int. Ed.*, 2025, **64**, e202500610.
14 Y. Zuo, X. Wang and D. Wu, *J. Mater. Chem. C*, 2019, **7**, 14555-14562.
15 R. Feng, H. Lv and Q. Song, *Angew. Chem. Int. Ed.*, 2026, **65**, e16177.
16 Z. Huang, Z. He, B. Ding, H. Tian and X. Ma, *Nat. Commun.*, 2022, **13**, 7841.
17 J. Yu, H. Yu, J. Niu, Z. Lei and Y. Liu, *Nano Letters*, 2024, **24**, 16124-16131.

18 H. Hu, X. Cheng, Z. Ma, Q. Yang, P. Sijbesma Rint and Z. Ma, *CCS Chem.*, 2023, **6**, 1798-1809.
19 Y. Huang, Y. Liu, X. Zheng, J. Wu, Q. Ling and Z. Lin, *Adv. Optical Mater.*, 2025, **13**, 2500743.
20 N. Li, X. Yang, B. Wang, P. Chen, Y. Ma, Q. Zhang, Y. Huang, Y. Zhang and S. Lü, *Adv. Sci.*, 2024, **11**, 2404698.
21 R. Liu, C. Liu, C. Fu, Z. Zhu, K. Chen, C. Li, L. Wang, Y. Huang and Z. Lu, *Angew. Chem. Int. Ed.*, 2024, **63**, e202312534.
22 H. Wu, D. Wang, Z. Zhao, D. Wang, Y. Xiong and B. Tang, *Adv. Funct. Mater.*, 2021, **31**, 2101656.
23 W. Wen, P. Ze, Z. Min and Q. Ming, *Chem. Eng. J.*, 2024, **495**, 153443.
24 R. Tian, S. Xu, Q. Xu and C. Lu, *Sci. Adv.*, 2020, **6**, eaaz6107.
25 Z. Xu, Y. Huang, S. Sun, P. Wang, Z. He, H. Tian, X. Ma. *Angew. Chem. Int. Ed.*, 2025, **64**, e202518340.
26 T. Heidi, P. Dominik L, G. Max, A. Tim, S. Annika, L. Marine, X. Feng and R. Sebastian, *Adv. Mater.*, 2020, **32**, 2000880.
27 X. Zhang, Z. Gong, J. Sun, M. Wang, X. Ding and H. Xu, *Angew. Chem. Int. Ed.*, 2026, **65**, e23525.
28 J. Li, J. Zhang, Y. Ju, Z. Zhou, S. Liu, Y. Ma and Q. Zhao, *Adv. Optical Mater.*, 2026, **14**, e02364.
29 Z. Chi, D. Li, Y. Meng, Z. Qiao, J. Yang, J. Zhou, X. Liu and Z. Li, *Sci. China Chem.*, 2026, **69**, 413-419.
30 S. Sun, L. Ma, J. Wang, X. Ma, H. Tian. *Natl. Sci. Rev.*, 2022, **9**, nwab085.
31 Z. Guan, Z. Tang, Z. Yao, Q. Guo, S. Zhang, Z. Lv, X. Zhang, N. Ma, X. Liu and Z. Hu, *Adv. Mater.*, 2025, **37**, e07192.
32 D. Li, J. Yang, M. Fang, B. Tang and Z. Li, *Sci. Adv.*, 2022, **8**, eabl8392.
33 G. Yang, S. Hao, X. Deng, X. Song, B. Sun, W. Hyun, M. Li and L. Dang, *Nat. Commun.*, 2024, **15**, 4674.
34 Y. Cai, Z. Wang, Y. Cui, X. Chen, G. Yang, H. Ou, H. Yuan and W. Yuan, *Adv. Mater.*, 2026, **38**, e18820.
35 W. Guo, X. Wang, B. Zhou and K. Zhang, *Chem. Asian J,* 2020, **15**, 3469-3474.
36 W. Hao, Y. Wang and M. Liu, *ACS Mater. Lett.*, 2024, **6**, 3487-3495.
37 Q. Wang, Q. Zhang, Q. Zhang, X. Li, C. Zhao, T. Xu, D. Qu and H. Tian, *Nat. Commun.*, 2020, **11**, 158.
38 A. Nicol, R. Kwok, C. Chen, W. Zhao, M. Chen, J. Qu and B. Tang, *J. Am. Chem. Soc.*, 2017, **139**, 14792-14799.
39 Y. Zhang, Y. Su, H. Wu, Z. Wang, C. Wang, Y. Zheng, X. Zheng, L. Gao, Q. Zhou, Y. Yang, X. Chen, C. Yang and Y. Zhao, *J. Am. Chem. Soc.*, 2021, **143**, 13675-13685.
40 M. Liu, B. Wu, S. Shen, H. Sun, X. Gu, S. Li, Z. Tang, J. Cheng, X. Ma, M. Zhang, Y. Xu and L. Zhu, *ACS Macro Lett.*, 2025, **14**, 93-100.
41 M. Wu, Y. Guan, P. Wang, T. Hao, J. Li, W. Yuan, J. Huang, P. Duan, P. Wang and H. Xie, *Adv. Funct. Mater.*, 2025, **35**, 2505113.
42 Y. Lei, W. Dai, Y. Tian, J. Yang, P. Li, J. Shi, B. Tong, Z. Cai and Y. Dong, *J. Phys. Chem. Lett.*, 2019, **10**, 6019-6025.
43 L. Zhou, S. Mu, L. Ma, P. Jiang, Z. He, J. Song and X. Ma, *ACS Mater. Lett.*, 2024, **6**, 5384-5391.
44 X. Yao, Z. Lin, X. Liu, H. Ma, X. Wang, W. Huang and Z. An, *Angew. Chem. Int. Ed.*, 2025, **64**, e202510153.
45 S. Jia, B. Yang, J. Zhang, Y. Zhang, J. Wei, J. Du, M. Shan, J. Tang, W. Tang and J. Gong, *Small*, 2025, **21**, 2505073.
46 H. Liang, L. Yang, J. Cheng, T. Li, D. Zhang and Z. Xu, *Adv. Funct. Mater.*, 2026, **36**, e13575.
47 C. Yang and B. Yan, *ACS Appl. Mater. Interfaces*, 2025, **17**, 34219-34229.
48 X. Piao, T. Wang, X. Chen, G. Wang, X. Zhai and K. Zhang, *Nat. Commun.*, 2025, **16**, 868.
49 H. Yang, Y. Wang, Y. Wang, Z. Zhang, H. Ma, Y. Yamauchi, K. Ling, Y. Zhao, S. Cai, Z. An and W. Huang, *Adv. Mater.*, 2025, **37**, e03550.
50 Z. Yin, Z. Wu and B. Liu, *Adv. Mater.*, 2025, **37**, 2506549.
51 Z. Deng, J. Zhang, J. Zhou, W. Shen, Y. Zuo, J. Wang, S. Yang, J. Liu, Y. Chen, C. Chen, G. Jia, P. Alam, J. W. Y. Lam and B. Z. Tang, *Adv. Mater.*, 2024, **36**, 2311384.
52 Z. Xu, Y. Huang, S. Sun, L. Ma, B. Ding, H. Tian, X. Ma. *Nature Commun.*, 2025, **16,** 9668.
53 C. Chen, Z. Chi, K. Chong, A. Batsanov, Z. Yang, Z. Mao, Z. Yang and B. Liu, *Nat. Mater.*, 2021, **20**, 175-180.
54 X. Bao, E. Ushakova, E. Liu, Z. Zhou, D. Li, D. Zhou, S. Qu and A. Rogach, *Nanoscale*, 2019, **11**, 14250-14255.
55 P. Jiang, B. Ding, J. Yao, L. Zhou, Z. He, Z. Huang, C. Yin, H. Tian and X. Ma, *Angew. Chem. Int. Ed.*, 2025, **64**, e202421036.
56 Y. Zhang, X. Chen, J. Xu, Q. Zhang, L. Gao, Z. Wang, L. Qu, K. Wang, Y. Li, Z. Cai, Y. Zhao and C. Yang, *J. Am. Chem. Soc.*, 2022, **144**, 6107-6117.
57 D. Wang, H. Wu, J. Gong, Y. Xiong, Q. Wu, Z. Zhao, L. Wang, D. Wang and B. Tang, *Mater. Horiz.*, 2022, **9**, 1081-1088.
58 G. Ye, Y. Yang, W. Yuan, J. Gu, S. Li, Q. Li and Z. Li, *ACS Mater. Lett.*, 2024, **6**, 4639-4648.
59 M. A. El‐Sayed, *J. Chem. Phys.*, 1963, **38**, 2834-2838.
60 X. Li, W. Li, Z. Deng, X. Ou, F. Gao, S. He, X. Li, Z. Qiu, R. Kwok, J. Sun, D. Phillips, J. Lam, Z. Guo and B. Tang, *J. Am. Chem. Soc.*, 2025, **147**, 14198-14210.
61 Y. Zhu, Y. Guan, Y. Niu, P. Wang, R. Chen, Y. Wang, P. Wang and H. Xie, *Adv. Optical Mater.*, 2021, **9**, 2100782.
62 H. Sun, Y. Xiao, Y. He, X. Wei, J. Zou, Y. Luo, Y. Wu, J. Zhao, V. Au and T. Yu, *Chem. Sci.*, 2025, **16**, 5299-5309.
63 J. Bai, L. Han, Y. Liu, L. Bu, S. Hu, J. Ma, Z. Li, M. Chen, Z. Ma and Z. Ma, *Adv. Funct. Mater.*, 2025, **35**, 2411496.

View Article Online
DOI: 10.1039/D6SC02475K

Data are available in Electronic Supplementary Information.